HET HOBBY ★ EBERLY TELESCOPE

HET Technical Report #42

Tracker Mechanism Kinematics, Servo, and Top-level Software Design for a Semi-transit Telescope with Fixed Spherical Primary Mirror

F. B. Ray

Hobby * Eberly Telescope Project
McDonald Observatory
University of Texas
RLM 15.308
Austin, Texas 78712

April 4, 1994

A Joint Project of
The University of Texas at Austin, The Pennsylvania State University,
Stanford University, Ludwig-Maximilians-Universität München, and Georg-August-Universität Göttingen

Tracker mechanism kinematics, servo, and top-level software design for a semi-transit telescope with fixed spherical primary mirror

F. B. Ray
The University of Texas McDonald Observatory
Austin, Texas 78712

Latest revision: June 24, 1994

1. Introduction

A large terrestrial telescope having a spherical primary mirror benefits from invariant gravitational deflections in the primary mirror structure. A corrector mounted near the prime focus may be driven to compensate for the earth's rotation to extend the transit period of an object across the usable field of the telescope. Physical (limitations of the tracking mechanism) and optical (vignetting of the entrance pupil) constraints put practical bounds on the mechanism's geometry, which are incorporated into the tracking control equations. Both equatorial and altitude-azimuth mounts have been proposed.

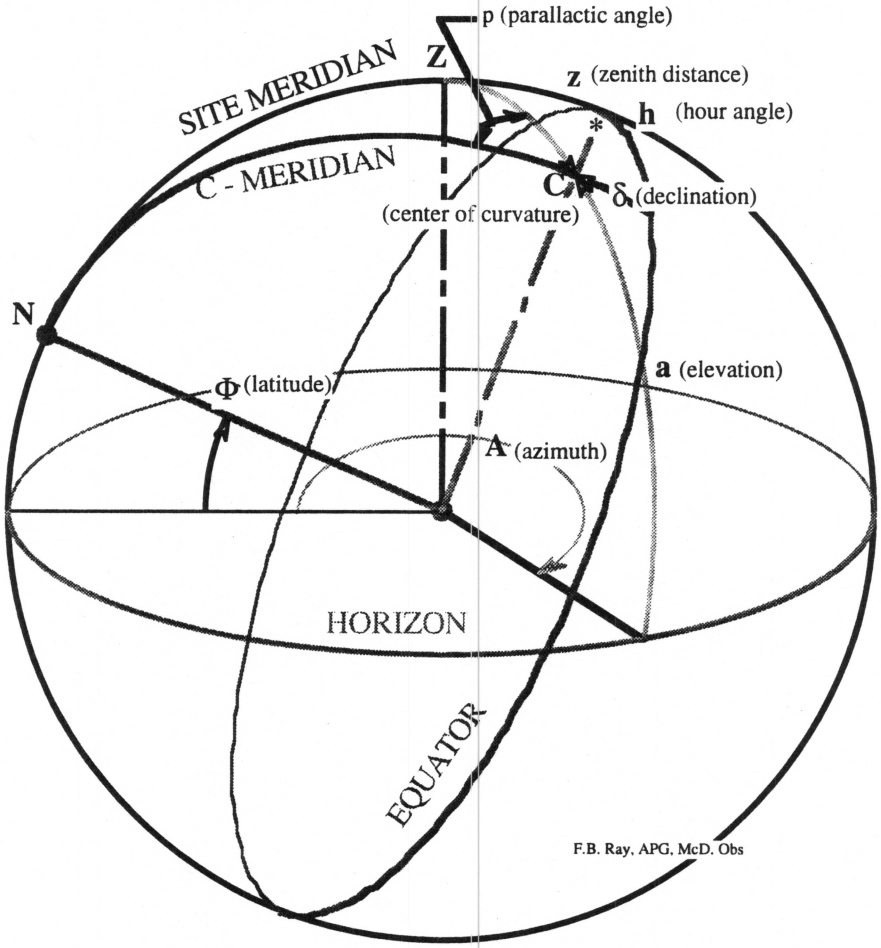

Figure 1.

Coordinates for SST center of curvature (alt.-az.)

An example of the latter is the University of Texas / Penn State University Spectroscopic Survey Telescope (SST), in which elevation is fixed at an angle of 55° from the horizon, image tracking is available 6° either side of the object's transit meridian, and all azimuths are available, but no azimuth tracking is performed. The operational mode is therefore to set the telescope in azimuth according to the

object's declination and intercept an image trajectory as it enters and migrates across the telescope's available hour angle reach. In a survey mode, the SST may observe objects in a declination band 12° wide.

A multi-axis tracking robot mounted at the upper end of the SST must perform all of the time-dependent motion control in order to follow an image trajectory in the vicinity of its transit. The variables examined may be used to develop control strategies and algorithms for the motion control of a multi-axis machine suitable for following an image trajectory. In addition, it may be seen that certain design opportunities exist which can provide for coma correction and the injection of astronomically meaningful and operator-supplied rate and position corrections.

Since the transformations describing the image trajectory and its projection into the gantry, or "tip" space are transcendental and involve several matrix multiplications, consideration must be given to whether these computations will conveniently fit into memory supplied with the controller hardware, or whether a distributed computing task, with core trajectory computations being performed in a host computer and associated I/O to the controller modules, might better serve the tracking function. The special nature of the SST optical arrangement creates certain favored modes of tracking correction, and tilt limits for the corrector help to form a partition for coarse and fine guiding corrections.[1]

Some mechanical engineering is necessary to determine the best tradeoffs in defining a center of rotation for the tracking robot (angular pointing). In this analysis, we define this point as the "rotation point", abbreviated **RP**. Tilting the corrector about (the correctly-tracked) point **RP** results in coincidence of the primary mirror's center of curvature with the line of sight, and is therefore equivalent to a rotation about the center of curvature.

2. Nomenclature

Group 1 – variables fixed by telescope geometry or Azimuth

Center of curvature (COC) – the center of the SST's spherical primary mirror
Polar axis – the axis of rotation, containing the center of curvature, parallel to the earth's pole
Telecentric axis – the axis defined by the vertex of the central mirror segment and the center of curvature
Tracking sphere – a particular sphere centered at the COC
Transit plane – the plane defined by the earth's polar axis and the SST's center of curvature
C-Meridian – the meridian coinciding with the transit plane
Transit time – the time at which the image crosses the transit plane
Transit point – the intersection of the image trajectory with the transit plane
Reach – an angular offset in declination from the telecentric axis
H – the angular distance from the telecentric axis to the site meridian
a – the angular distance from the telecentric axis to the horizon (elevation)
Z – the angular distance from the telecentric axis to the local zenith (zenith angle)
Φ – latitude of the SST
$\mathbf{p_c}^*$ – principal value of the parallactic angle of the tracking mechanism
$\mathbf{p_c}$ – parallactic angle of the tracking mechanism (rotation about the telecentric axis, also denoted by **pa**)
δ_T – angular distance from the transit point to the equator, or declination at time of transit
δ_c – angular distance from the telecentric axis to the equator (also known as **TDE**)
A – azimuth, measured clockwise from north (East is 90°)
$\mathbf{F_S}$ – radius of the tracking sphere
$\mathbf{F}^*$ – radius of the sphere centered at the COC and containing the coma correction node

Group 2 – time-varying quantities (device independent)

rotation point (RP) - the point tracked by the Cartesian (XYZ) mechanism
t – sidereal time
$\mathbf{h_c(t)}$ – hour angle with respect to the transit plane (may be non-linear)
δ**(t)** – declination of the object (not, in general, constant)
β**(t)** – the angle between the telecentric axis and the line of sight maintained by the tracker

---

1 P. MacQueen, "SST Optical Report", SST Technical Report TR-055, summer, 1991.

m(t) – angular length of the trajectory
ω**(t)** – the angle between the great circle containing the telecentric axis and **RP** and the transit plane
ρ**(t)** – field rotation induced by the tracking displacement
r(t) – distance from **RP** to the transit plane
d(t) – distance to the projection of **RP** in the transit plane from the telecentric axis
x(t) – distance of **RP** from the Y-axis of an XYZ mechanism whose XY plane is perpendicular to the telecentric axis
y(t) – distance of **RP** from the X-axis of an XYZ mechanism whose XY plane is perpendicular to the telecentric axis
z(t) – distance from the plane tangent to the tracking sphere at its vertex to **RP**
θ**(t)** – projected angle of the line of sight in the YZ plane of an XYZ mechanism whose XY plane is perpendicular to the telecentric axis
ϕ**(t)** – projected angle of the line of sight in the XZ plane of an XYZ mechanism whose XY plane is perpendicular to the telecentric axis

Group 3 – special variables and constants associated with a "wobble plate" tracking mechanism

r_{WP} – radius of 3 parallel precision screw legs
x(t) – linear displacement parallel to the X-axis of the tracker mechanism
y(t) – linear displacement parallel to the Y-axis of the tracker mechanism
L1(t) – linear displacement of tilt table leg 1
L2(t) – linear displacement of tilt table leg 2
L3(t) – linear displacement of tilt table leg 3
ρ**(t)** – parallactic angle and field rotation of an instrument rotator

Group 4 – special variables and constants associated with a "hexapod" tracking mechanism

x(t) – linear displacement parallel to the X-axis of the tracker mechanism
y(t) – linear displacement parallel to the Y-axis of the tracker mechanism
H1(t) – linear displacement of hexapod leg 1
H2(t) – linear displacement of hexapod leg 2
H3(t) – linear displacement of hexapod leg 3
H4(t) – linear displacement of hexapod leg 4
H5(t) – linear displacement of hexapod leg 5
H6(t) – linear displacement of hexapod leg 6
$\mathbf{p_c}$ – parallactic angle of the tracking mechanism (rotated & locked instrument plate)
ρ**(t)** – parallactic angle and/or field rotation of an instrument rotator

3. Basic equations

Given azimuth A, we can readily compute δ_c, **H**, and $\mathbf{p_c}^*$ as functions of **A** from the spherical triangles in figure 1. Azimuth is measured in the navigational sense, that is positive to the east from north. Elevation **a** is measured from the horizon.

$$\delta_c = \sin^{-1} [\cos \mathbf{a} \cos \Phi \cos \mathbf{A} + \sin \mathbf{a} \sin \Phi] \tag{1}$$

$$\mathbf{H} = \sin^{-1} \left[\frac{\cos \mathbf{a} \sin \mathbf{A}}{-\cos \delta_c} \right] \tag{2}$$

Variables δ_c and **H** are plotted versus azimuth in figure 2. Parallactic angle, principal value, is

$$\mathbf{p_c}^* = \cos^{-1} [\cos \mathbf{H} \cos \mathbf{A} + \sin \mathbf{H} \sin \mathbf{A} \sin \Phi] \tag{3}$$

The cosine form of $\mathbf{p_c}^*$ given by equation 3 contains a discontinuity in the first derivative at $\mathbf{A} = \pi$, but the tangent form for $\mathbf{p_c}^*$ usually employed for alt-az coordinate transformations has two discontinuities. The plot in figure 3 illustrates the efficacy of using the cosine form in producing a workable function for **p** analytic in the half-open interval $[0,2\pi)$.The functions **H** and δ_c are plotted in figure 2, using the latitude of McDonald Observatory at Ft. Davis, Texas ($\approx$30.6716°) and an assumed SST elevation angle of 55°.

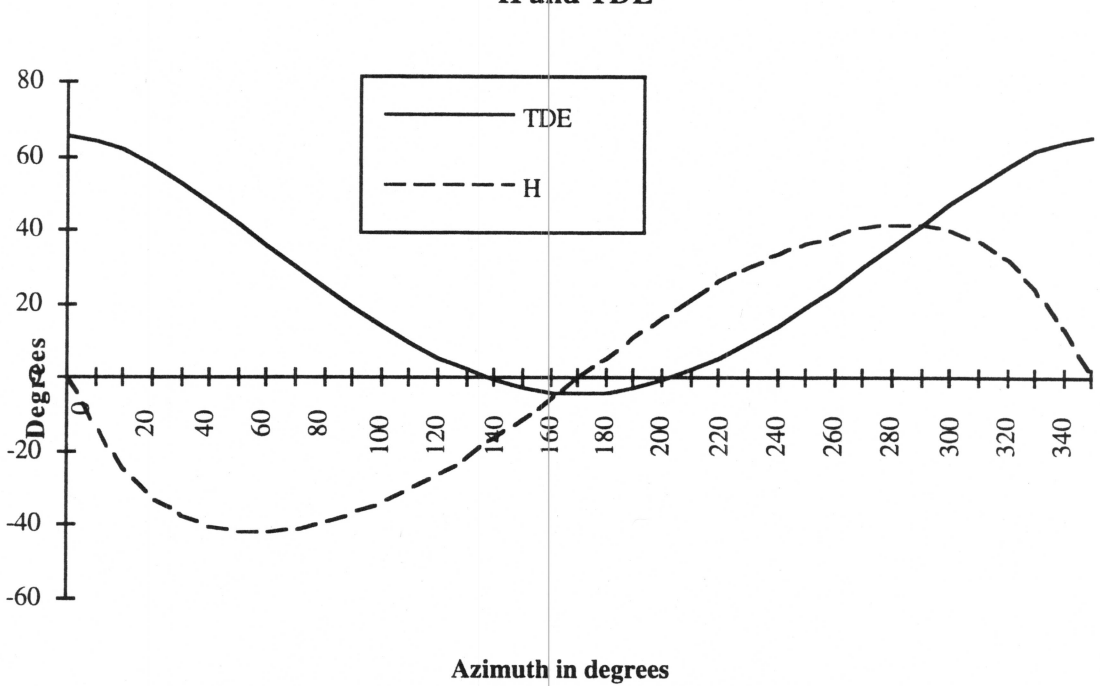

Figure 2. Distance of the SST's telecentric axis to the equator (**TDE** = δ_c) and to the meridian (**H**).

In figure 3 the parallactic angle for the tracking device is plotted against azimuth for both equation 3 and an alternate (tangent) form usually given in astrometric reference texts.[2] To create the continuous parallactic angle function $\mathbf{p_c}$, depicted by PA2 in the graph, which is analytic in the half-open interval $[0,2\pi)$, we have to deal with a slope discontinuity at π, as follows:

$$\mathbf{p_c} = \begin{cases} \mathbf{p_c}^* \text{ , if } 0 \le \mathbf{A} \le \pi \\ 2\pi - \mathbf{p_c}^* \text{ , otherwise} \end{cases} \tag{4}$$

Similar to that provided for the azimuth axis, a service loop for flexible conductors must be provided for parallactic angle rotation, and safety limits of parallactic rotation should therefore be maintained. Field rotation while tracking may be serviced by the same loop, since its range is much smaller for a typical image trajectory. An engineering decision concerning azimuth excursions greater than 360° is necessary to determine whether the parallactic angle rotation will be continuous at 360° or "retract" and start from 0°. The same tradeoff can also be considered at **A** = 180°. This may depend on limits for service loops, available space, etc.

2 Lang, K. R., *Astrophysical Formulae*, p. 503, Springer-Verlag, 1974, supplies the relationship

$$p = \tan^{-1}\left[\frac{\sin h}{\tan \phi \cos \delta - \sin \delta \cos h}\right]$$

for the principal value of the parallactic angle p, for example.

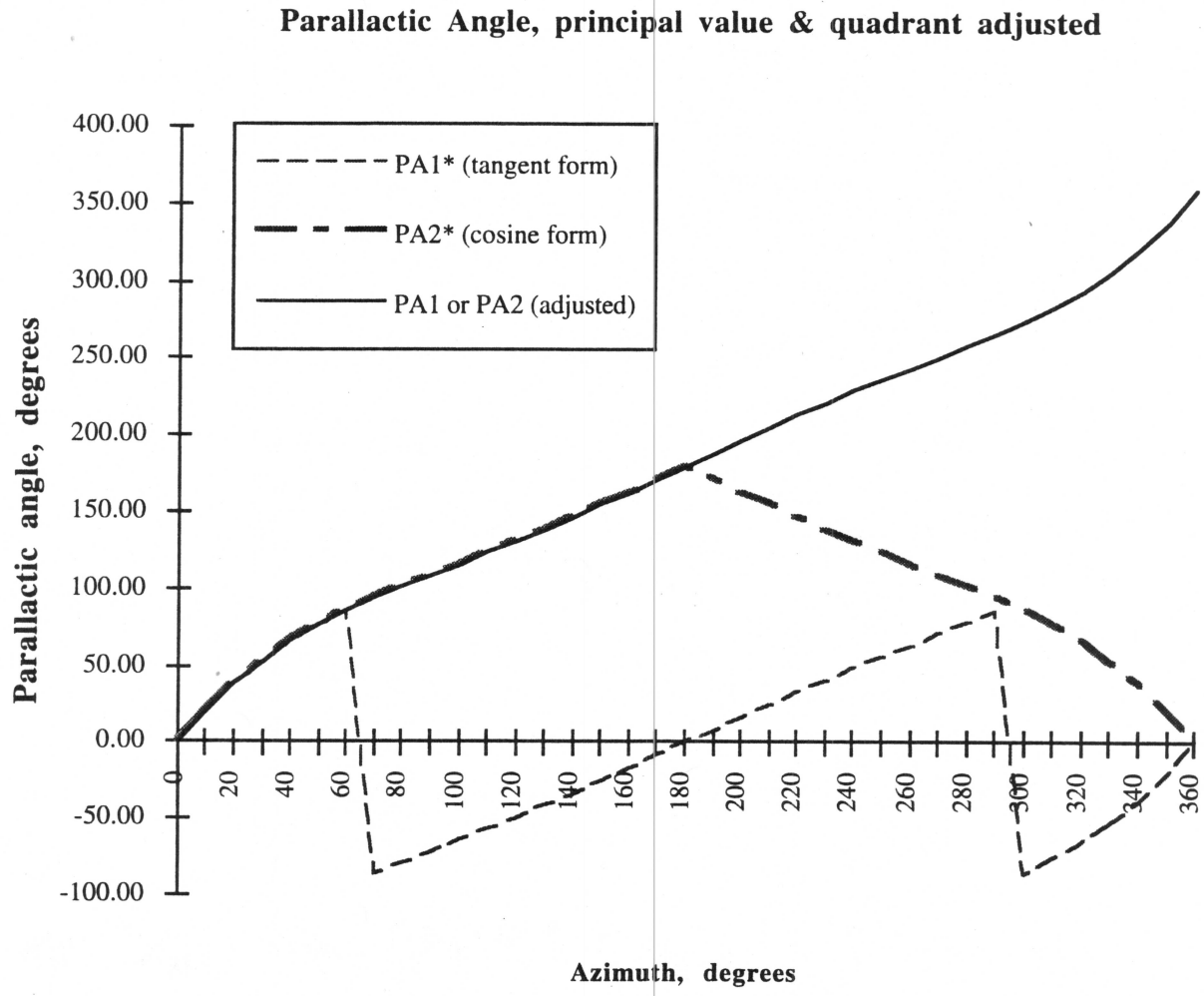

Figure 3. Parallactic angle of the SST's tracking mechanism. The principal value of the cosine form PA2* has fewer discontinuities in the first derivative. It is therefore easier to form a function for the parallactic angle which is useful for servomechanism control (analytic over the azimuth half-open interval $[0,2\pi)$).

On the tracking sphere, whose radius $\mathbf{F}_S$ is approximately equal to the optical system's focal length, we may establish spherical triangles as shown in figure 4 to illustrate the derivation of time-dependent tracking quantities for **RP**'s trajectory. Point **RP** in the figure is the (tracked) rotation point, **C** is the intersection of the telecentric axis with the tracking sphere, and N is the north pole on the tracking sphere. A "line of sight" joining the center of curvature (**COC**) and point **RP**, not shown in figure 4, makes an angle β with the telecentric axis. Both hour angle from transit $\mathbf{h_c}(t)$ and declination $\delta(t)$ are free parameters which may be varied according to any available ephemeris.

The **RP** trajectory has arc length

$$\mathbf{m}(t) = \mathbf{h_c}(t)\, \mathbf{F}_S \cos \delta(t) \tag{5}$$

and the angular distance of **RP** from the telecentric axis is

$$\beta(t) = \cos^{-1} [\sin \delta_{\mathbf{c}} \sin \delta(t) + \cos \delta_{\mathbf{c}} \cos \delta(t) \cos \mathbf{h_c}(t)] \tag{6}$$

The trajectory **RP** is a circle when declination is constant, but is not, in general, a great circle.

The rotation of the line of sight about the telecentric axis $\omega(t)$ is given by

$$\omega(t) = \begin{cases} \sin^{-1}\left[\dfrac{\sin \mathbf{h_c}(t) \cos \delta(t)}{\sin \beta(t)}\right], \text{ if } \beta(t) > 0 \\ 0, \text{ otherwise} \end{cases} \quad (7)$$

As hour angle varies, the symmetric field rotation $\rho(t)$ which matches the sense of the parallactic angle is

$$\rho(t) = -\sin^{-1}(\sin \delta(t) \sin \mathbf{h_c}(t)) \quad (9)$$

which therefore may be algebraically added to the parallactic angle **p** to give an analytic function for field rotation relative to the instrument rotator's zero encoder position (presumed to be 0° when **A** = 0°). If declination is not constant, the symmetric field rotation is non-linear.

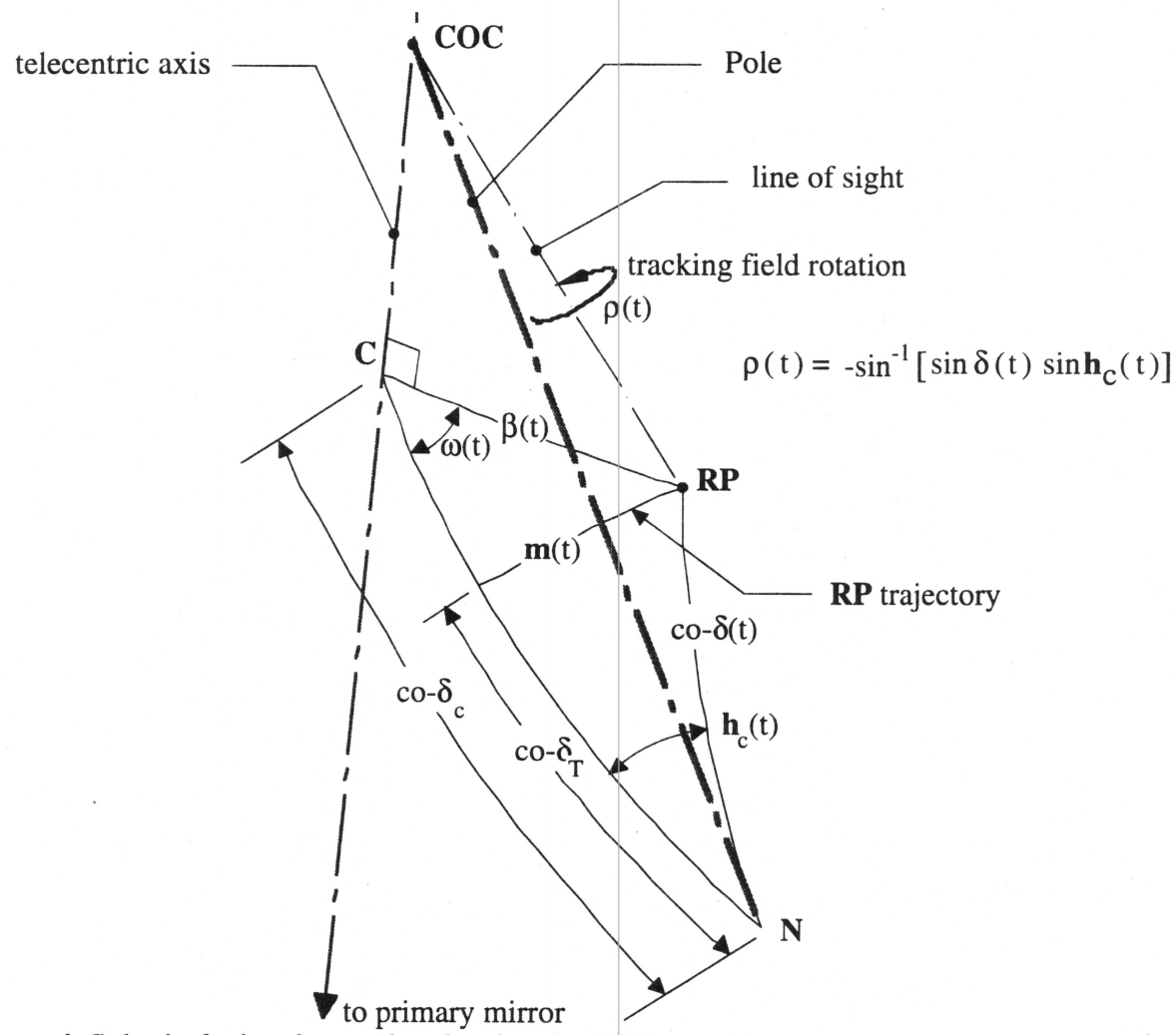

Figure 4. Spherical triangles used to develop the SST's tracking variables. The notation co-**x** is an abbreviation for the complementary angle of **x**, or 90° - **x**. The **RP** trajectory does not, in general, lie along a great circle, although that is the case when $\delta_T = 0$ and declination is constant. Point **C** is the intersection of the telecentric axis with the tracking sphere. **N** is the north pole on the tracking sphere, and **RP** is the (tracked) rotation point. For SST tracking, transit hour angle $\mathbf{h_c}(t)$ is measured from the transit plane, which contains **N** and **C**. The **RP** trajectory and field rotation are symmetric with the transit plane.

4. Cartesian (gantry) equations

For telescopes of the SST type, a gantry-based (XYZ) tracking mechanism has been proposed as the fundamental generator for the space curves necessary to follow a trajectory on the tracking sphere. In order to maintain a normal orientation of the optics, additional mechanism is added to provide 2-axis tilt

about the center of curvature of the primary mirror. Prime focus spectrometer apertures also require correction for field rotation as a rotation point is tracked across the available gantry space, and the optical corrector near prime focus benefits from 2-axis tip/tilt freedom about an optical node for coma correction and fine guiding (the "coma-neutral" node). We therefore must project the space curve marked "**RP** trajectory" in figure 4 to a Cartesian coordinate system related to the gantry mechanism and the tilt mechanisms it carries.

Relating the above spherical tracking triangles to a Cartesian coordinate system fixed to the telescope's upper surface, we require several auxiliary variables. First, we define 2D rectangular coordinates (**r**,**d**) for a system whose **R** axis is perpendicular to the transit plane, as

$$\mathbf{r}(t) = \mathbf{F}_S \cos \delta(t) \sin \mathbf{h_c}(t) \tag{10}$$

$$\mathbf{d}(t) = \mathbf{F}_S [\sin (\delta_T - \delta_c) + \sin \delta_c (\cos \delta_T - \cos \delta(t) \cos \mathbf{h_c}(t))] \tag{11}$$

which is of the form

$$\mathbf{d}(t) = \mathbf{F}_S [C5 - C2 \cos \delta(t) \cos \mathbf{h_c}(t)] \tag{12}$$

if

$$C1 = \sin (\delta_T - \delta_c),\ C2 = \sin \delta_c,\ C3 = \cos \delta_T,\ C4 = C2\ C3,\ \text{and}\ C5 = C1 + C4 \tag{13}$$

and $\mathbf{F}_S$ is the radius of the tracking sphere.

Then, with a parallactic rotation $\mathbf{p_c}$ about the telecentric axis, we obtain **x** and **y**, coordinates in a hypothetical mechanism's X and Y (mechanical) directions,

$$\mathbf{x}(t) = \mathbf{r}(t) \cos \mathbf{p_c} - \mathbf{d}(t) \sin \mathbf{p_c} \tag{14}$$

$$\mathbf{y}(t) = \mathbf{r}(t) \sin \mathbf{p_c} + \mathbf{d}(t) \cos \mathbf{p_c} \tag{15}$$

Projection angles $\theta(t)$ and $\phi(t)$ related to the tracker's Cartesian coordinate system are then

$$\theta(t) = \tan^{-1}\left[\frac{\mathbf{y}(t)}{\mathbf{F}_S \cos \beta(t)}\right] \tag{16}$$

$$\phi(t) = \tan^{-1}\left[\frac{\mathbf{x}(t)}{\mathbf{F}_S \cos \beta(t)}\right] \tag{17}$$

The displacement parallel to the telecentric axis we define as **z**(t) (also called the tracking sagitta), given by

$$\mathbf{z}(t) = \mathbf{F}_S [1 - \cos \beta(t)] = \mathbf{F}_S - \sqrt{\mathbf{F}_S{}^2 - \mathbf{x}(t)^2 - \mathbf{y}(t)^2} \tag{18}$$

5. Equations for an XYp+wobble plate tracking mechanism

A wobble plate, or tilt table mechanism mounted on top of an XY stage may provide **Z** motion and universal tilt about **RP** by varying the lengths (**L1**, **L2**, **L3**) of its 3 parallel legs. We will assume a set of 3 parallel precision screws which are fixed in bearings and are non-collinear. Other parallel screws may be incorporated as well, for a more stable non-kinematic platform; their length coordinates are computed in exactly the same inverse manner as for the simplest case of 3 legs. Parallactic and field rotation may be tracked by a rotating mechanism carried by the wobble plate. This mechanism induces coupled offsets in **X** and **Y** as its tilt changes, which must be corrected by the XY stage beneath.

Point **RP** is at an angle β to the telecentric axis, and may be defined by transforming, with a pure rotation, the vertex of the tracking sphere to **RP**. The matrix **R3** which performs this transformations formed from the following product of two matrices in homogeneous form, **RX** and **RY**, that is,

$$[\mathbf{R3}] = [\mathbf{RX}]\ [\mathbf{RY}] \tag{19}$$

where **RX** rotates points about the X axis by the angle

$$\zeta(t) = \sin^{-1}\left[\frac{\mathbf{y}(t)}{\mathbf{RV}_{YZ}(t)}\right],\ \left(\mathbf{RV}_{YZ}(t) = \sqrt{\mathbf{y}(t)^2 + (\mathbf{F}_S - \mathbf{z}(t))^2}\right), \tag{20}$$

and is defined as

$$[\mathbf{RX}] = \begin{bmatrix} 1 & 0 & 0 & 0 \\ 0 & \cos\zeta(t) & -\sin\zeta(t) & 0 \\ 0 & \sin\zeta(t) & \cos\zeta(t) & 0 \\ 0 & 0 & 0 & 1 \end{bmatrix}; \tag{20a}$$

similarly, **RY** rotates points about the Y axis by the angle $\psi(t) = \sin^{-1}\left[\frac{\mathbf{x}(t)}{\mathbf{F_S}}\right]$, and is defined by

$$[\mathbf{RY}] = \begin{bmatrix} \cos\psi(t) & 0 & -\sin\psi(t) & 0 \\ 0 & 1 & 0 & 0 \\ \sin\psi(t) & 0 & \cos\psi(t) & 0 \\ 0 & 0 & 0 & 1 \end{bmatrix}. \tag{21}$$

The signs of angles $\zeta(t)$ and $\psi(t)$ are the same as $\mathbf{x}(t)$ and $\mathbf{y}(t)$, respectively. Note that **RX** and **RY** are in transformational form, i.e. they transform points to a new position. Since it may be applied about any center or rotation, matrix **R3** is exactly the matrix needed to bring a tilting device's axis into coincidence with the primary mirror normal, in addition to being translated to the rotation point **RP**.

Various simplifications using selected identities can eliminate the trigonometric functions from the above matrices, for example,

$$[\mathbf{RX}] = \begin{bmatrix} 1 & 0 & 0 & 0 \\ 0 & \sqrt{\frac{\mathbf{y}(t)^2}{\mathbf{RV}_{YZ}(t)}} & \frac{-\mathbf{y}(t)^2}{\mathbf{RV}_{YZ}(t)} & 0 \\ 0 & \frac{\mathbf{y}(t)^2}{\mathbf{RV}_{YZ}(t)} & \sqrt{\frac{\mathbf{y}(t)^2}{\mathbf{RV}_{YZ}(t)}} & 0 \\ 0 & 0 & 0 & 1 \end{bmatrix} \tag{21a}$$

and

$$[\mathbf{RY}] = \begin{bmatrix} \sqrt{1-\frac{\mathbf{x}(t)^2}{\mathbf{F_S}^2}} & 0 & \frac{-\mathbf{x}(t)}{\mathbf{F_S}} & 0 \\ 0 & 1 & 0 & 0 \\ \frac{\mathbf{x}(t)}{\mathbf{F_S}} & 0 & \sqrt{1-\frac{\mathbf{x}(t)^2}{\mathbf{F_S}^2}} & 0 \\ 0 & 0 & 0 & 1 \end{bmatrix}, \tag{21b}$$

which should enhance real-time computation, but for clarity it's best to express such matrices in their trigonometric rotational form. Computation of feed-forward servo position information and stabilization rates may be enhanced by reducing the string of matrix computations to the simplest level possible.

Multiplication by matrix **R3** rotates the wobble plate such that the normal to the wobble plate is parallel to the line of sight. In order to achieve this rotation on 3 parallel screws, we also must compute the screw displacements equivalent to a multiplication by matrix **R3**. The vectors {W1} = {0,0,0,1}, {W2} = {1,0,0,1}, and {W3} = {0,1,0,1} represent 3 non-collinear points in the plane of the wobble plate (note the use of homogeneous coordinates to allow the construction of a translation matrix). The XY coordinates of the 3 parallel screws (fixed by bearings) are represented by the points $(x1_S,y1_S)$, $(x2_S,y2_S)$, $(x3_S,y3_S)$. Our problem is to solve for the Z displacements of the 3 screws.

The center of rotation (normally the point **RP**) may now be defined relative to the wobble plate center, and denoted by the vector **CF** = $\{x_c,y_c,z_c,1\}$. We define a translation matrix **T1** to place **CF** at the center of rotation as

$$[\mathbf{T1}] = \begin{bmatrix} 1 & 0 & 0 & -x_c \\ 0 & 1 & 0 & -y_c \\ 0 & 0 & 1 & -z_c \\ 0 & 0 & 0 & 1 \end{bmatrix} \tag{22}$$

Using the rotation **R3**, we compute the rotational transforms after translation of {W1}, {W2}, and {W3} as

$$\{x1,y1,z1,1\}^T(t) = [\mathbf{T1}]^{-1}[\mathbf{R3}]\,[\mathbf{T1}]\,\{W1\}^T \tag{23}$$

$$\{x2,y2,z2,1\}^T(t) = [\mathbf{T1}]^{-1}[\mathbf{R3}]\,[\mathbf{T1}]\,\{W2\}^T \tag{24}$$

$$\{x3,y3,z3,1\}^T(t) = [\mathbf{T1}]^{-1}[\mathbf{R3}]\,[\mathbf{T1}]\,\{W3\}^T \tag{25}$$

which all must lie in the plane parallel to one with equation

$$Ax + By + Cz + D = 0 \tag{26}$$

where A, B, C and D are all functions of time, but here (t) is omitted from the equations, and

$$A = (y2 - y1)(z3 - z1) - (z2 - z1)(y3 - y1) \tag{27}$$

$$B = (z2 - z1)(x3 - x1) - (x2 - x1)(z3 - z1) \tag{28}$$

$$C = (x2 - x1)(y3 - y1) - (y2 - y1)(x3 - x1) \tag{29}$$

$$D = -(Ax1 + By\,1 + Cz1) \tag{30}$$

The ends of the parallel screws must also lie in this plane, hence their displacements are computed from their fixed XY coordinates as

$$z1_s(t) = \frac{-(Ax1_s + By1_s + D)}{C} \tag{31}$$

$$z2_s(t) = \frac{-(Ax2_s + By2_s + D)}{C} \tag{32}$$

$$z3_s(t) = \frac{-(Ax3_s + By3_s + D)}{C} \tag{33}$$

The wobble rotation induces Cartesian offsets of points other than the wobble center of rotation. Let the vector $\mathbf{CC} = \{x_c,y_c,z_c\}$ represent the coordinates of another point relative to the wobble plate (such as the center of curvature). Transformation of the corrected focus {FP} by $[\mathbf{T1}]^{-1}[\mathbf{R3}][\mathbf{T1}]$, i.e.

$$\{DFX,DFY,DFZ,1\}^T(t) = [\mathbf{T1}]^{-1}[\mathbf{R3}]\,[\mathbf{T1}]\,\mathbf{CC}^T \tag{34}$$

for example, gives the displacements {DFX,DFY,DFZ} to be compensated by the X and Y mechanisms, where a constant displacement by all 3 parallel screws simultaneously compensates for DFZ. Formation of a translation matrix **[T2]** to shift the center of rotation to such a point will likewise induce Cartesian offsets at the corrected focus.

Note that it is not possible to rotate the wobble plate without inducing these offsets for points other than the wobble plate center of rotation. We can, however, eliminate Cartesian offsets from a single center of rotation.

To eliminate Cartesian offsets from rotations about **RP**, we assume **RP** is at the center of wobble plate rotation, whose direction must match the line of sight's, and the equations for **x** and **y** motion are as computed previously, or

$$\mathbf{x}(t) = \mathbf{r}(t)\cos\mathbf{p_c} - \mathbf{d}(t)\sin\mathbf{p_c} \tag{35}$$

$$\mathbf{y}(t) = \mathbf{r}(t)\sin\mathbf{p_c} + \mathbf{d}(t)\cos\mathbf{p_c} \tag{36}$$

where in the projection of equations 10 and 11, $\mathbf{F_S}$ is equal to the distance from the center of curvature to the corrected focus, as are the displacements for the 3 parallel screws, and we have, with **z**(t) from equation 16, the lengths of the legs

$$\mathbf{L1}(t) = \mathbf{z}(t) + z1_s(t) \tag{37}$$

$$\mathbf{L2}(t) = \mathbf{z}(t) + z2_s(t) \tag{38}$$

$$\mathbf{L3}(t) = \mathbf{z}(t) + z3_s(t) \tag{39}$$

with parallactic angle $\mathbf{p_c}$ given by equation (4) and tracking field rotation given by equation (9).

In this coupled situation, "hand paddle" corrections in hour angle and declination settings must percolate down through the entire set of coordinate computations, in order to correct the offsets in the XY stage. There is no convenient algorithmic "slot" where one might introduce corrector optics rotation about an optical node point, say, for the purpose of "coma-neutral" correction (independent of image centroid motion).

6. Equations for an XYp+hexapod tracking mechanism

The Stewart Platform, or "hexapod" mechanism commonly used for flight simulators and universal positioning applications, also provides a solution to tracking **RP**'s trajectory with the proper tilt.[3] Three points of a fixed plate are connected by 6 linear actuators to 3 points of a movable plate, to which the corrector mechanism, rotator, and instrument are attached (see figure 8). Since we know the inverse kinematics to be obeyed (based on the **RP** trajectory), it is possible to compute the real-time variation for a hexapod's 6 linear actuators. Because the hexapod allows independent rotation about any arbitrary axis, within the limits of its travel, small corrections for tracking errors, focus and field rotation may be made entirely by changes in the linear actuators of the local mechanism, without the necessity of inducing coupled corrections in the large underlying XY stage.

We will assume some slight mechanical separation of the 3 structural points on the fixed and movable plates of the hexapod, and assume there are 6 points in each hexapod plane, listed as follows:

fixed plate:

$Fj = \{xFj, yFj, zFj\}$, $j = 1,2,...,6$

movable plate (home position):

$Mj = \{xMj, yMj, zMj,1\}$, $j = 1,2,...,6$

If $\{CF\} = \{x_c,y_c,z_c,1\}$ represents the relative location of **RP** as previously, but now in the coordinate system centered on the hexapod's movable plate, then the same transformation used previously may be used to correct the points Mj for normal orientation at time t by the following set of multiplications:

$$\{Mj'\}^T = \{xMj', yMj', zMj',1\}^T(t) = [\mathbf{T1}]^{-1}[\mathbf{R3}]\,[\mathbf{T1}]\,\{Mj\}^T\,,\ j = 1,2,...,6 \qquad (40)$$

Similarly, z displacement defined by equation 18 may be introduced via a homogeneous translation matrix

$$[\mathbf{TZ}] = \begin{bmatrix} 1 & 0 & 0 & 0 \\ 0 & 1 & 0 & 0 \\ 0 & 0 & 1 & \mathbf{z}(t) \\ 0 & 0 & 0 & 1 \end{bmatrix} \qquad (41)$$

so that a first-order trajectory for the hexapod points is finally

$$\{Mj'\}^T = \{xMj', yMj', zMj',1\}^T(t) = [\mathbf{TZ}][\mathbf{T1}]^{-1}[\mathbf{R3}]\,[\mathbf{T1}]\,\{Mj\}^T\,,\ j = 1,2,...,6 \qquad (42)$$

whereupon the 6 required strut lengths may be computed as the Euclidean distance between appropriate points in the fixed and movable plates, i.e.

$$\mathbf{Hj}(t) = \sqrt{(xFj - xMj')^2 + (yFj - yMj')^2 + (zFj - zMj')^2}\ ,\ j = 1,2,...,6 \qquad (43)$$

This function may be readily distributed among the six controller CPUs for parallel computation.

In a more general form, all small corrections, including field rotation, focus, autoguiding and/or handpaddle corrections, and coma correction may be introduced as independent matrix factors without coupling to the underlying XY stage, by similarly defining the matrices **Q1**, **Q2**, **Q3**, and **Q4** as follows:

Q1: rotation about the line of sight (field rotation)

Q2: translation along the line of sight (focus)

---

3 see, for example, "Modeling and simulation of a Stewart platform type parallel structure robot", by G. K. Lim, M. S. Thesis, Univ. of Texas at Austin, May, 1988.

Q3: rotation about the COC (HA and dec. correction)

Q4: rotation about the coma-neutral node (up to about 0.6 arc seconds on the sky)

All of these are applied as multipliers of Mj to obtain the trajectory for attachment points in the hexapod's movable plate, in the form

$$\{Mj'\}^T = [\mathbf{Q1}][\mathbf{Q2}][\mathbf{Q3}][\mathbf{Q4}][\mathbf{TZ}][\mathbf{T1}]^{-1}[\mathbf{R3}]\ [\mathbf{T1}]\ \{Mj\}^T,\ j = 1,2,...,6 \qquad (44)$$

and equation 43 is employed to compute the individual leg positions in (possibly distributed) hardware.

Since transformations **Q1**, **Q2**, **Q3**, and **Q4** are applied only to the hexapod's movable plate, they do not introduce offsets in the XYZ mechanism below. This creates a mathematical foundation for an object-oriented interface suitable for the introduction of correction signals in the controlling software.

7. Image tracking strategies

If we assume that the image drifts from the normal, one strategy of correction is shown in figure 5, where the corrector optics are rotated about the COC and focused to make the correction.

This works well if the nature of the error is a tilt of the optic about the COC, and not so well, as shown in figure 5B, when the error derives from a more general tilt and/or translation. Figure 6A illustrates a shift of the exit aperture of the corrector away from the image due to a rotation about the coma-neutral node, which, according to P. MacQueen introduces only about 0.02 arc seconds of coma and no field curvature per arc second of rotation in the $D_{0.5}$ encircled energy error budget.[4] The SST error budget sets a maximum allowable rotation of this nature of about 7 arc seconds, which corresponds to a $D_{0.5}$ image error budget term of about 0.14 arc seconds.

On the sky, such errors are de magnified by the ratio L/F_S, where F_S is the radius of the focal sphere and L is the distance from the corrected focus to the coma-neutral node. This ratio is about 0.08 for the current SST design, which means that the 7 arc second range allowed translates to about 0.6 arc seconds on the sky. For mechanisms of roughly 1m dia., it will be shown later that this mode of correction and fine guiding reduces the precision required by the tilt linear actuators.

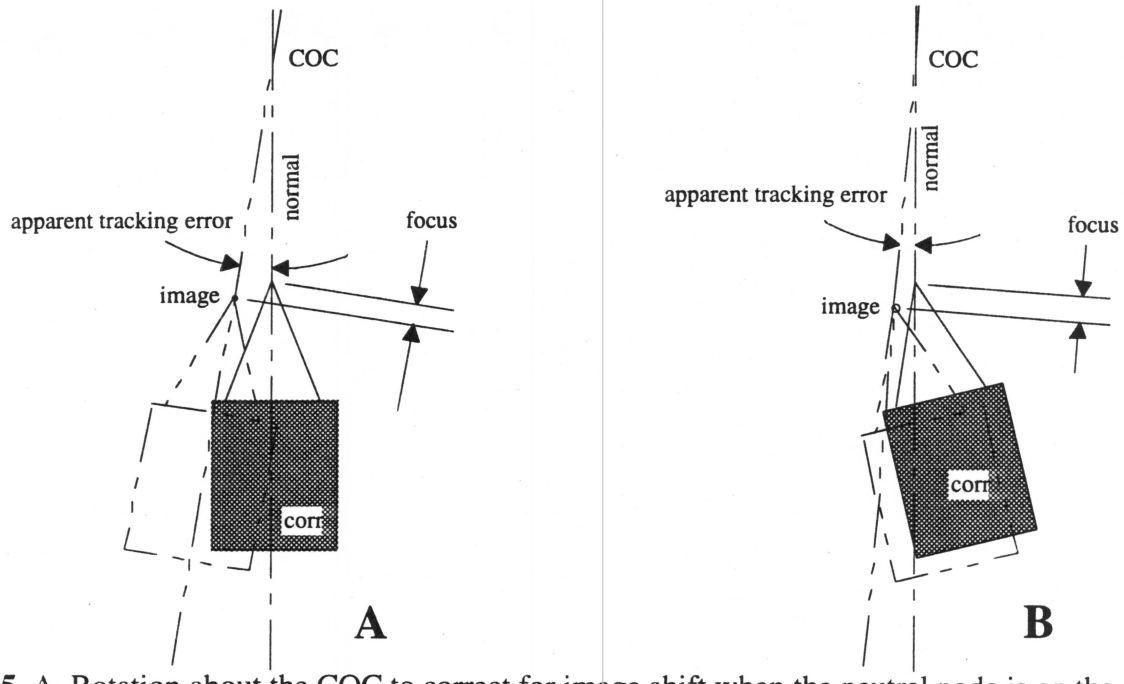

Figure 5. A. Rotation about the COC to correct for image shift when the neutral node is on the normal. B. Rotation about the COC to correct for image shift when the neutral node is not on the normal.

4 P. MacQueen, "SST Optical Report", SST Technical Report TR-055, summer, 1991.

Thus, one strategy for correcting drift errors of up to 0.6 arc seconds is to tilt the corrector optics up to 7 arc seconds about the coma-neutral node, as shown in figure 7a. Because this technique has limitations on the sky, an error budget for tracking the coma-neutral node may be established (to less than 0.5 arc seconds) to insure that the optics rotation will do the fine correction. This suggests tracking the coma-neutral node to an accuracy of 0.5 arc seconds, adjusting the tracking sphere radius $\mathbf{F}_S$ to suit that situation, and partitioning the guiding corrections into coarse (> 0.5 arc seconds) and fine (< 0.6 arc seconds.

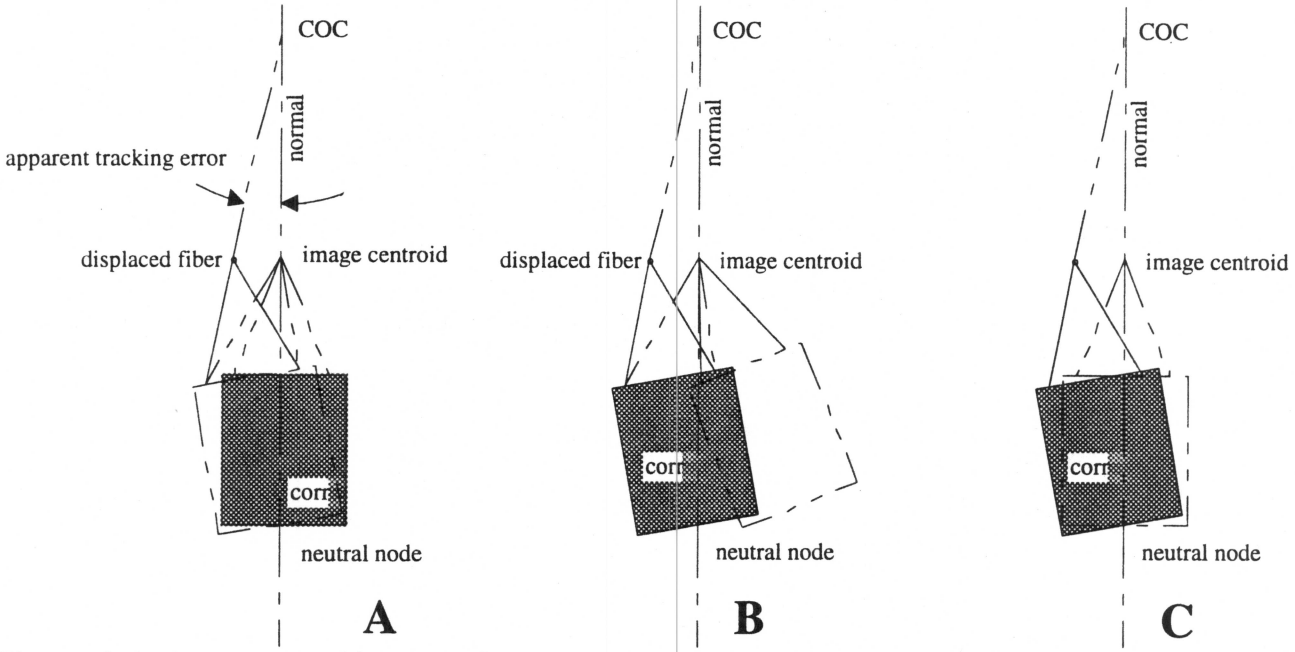

Figure 6. A. Apparent tracking error from a rotation of corrector optics and corrected focus about the coma-neutral optical node B. Rotation about the COC to correct for the image shift in part A. C. Correction of the image shift by counter-rotation about the neutral node.

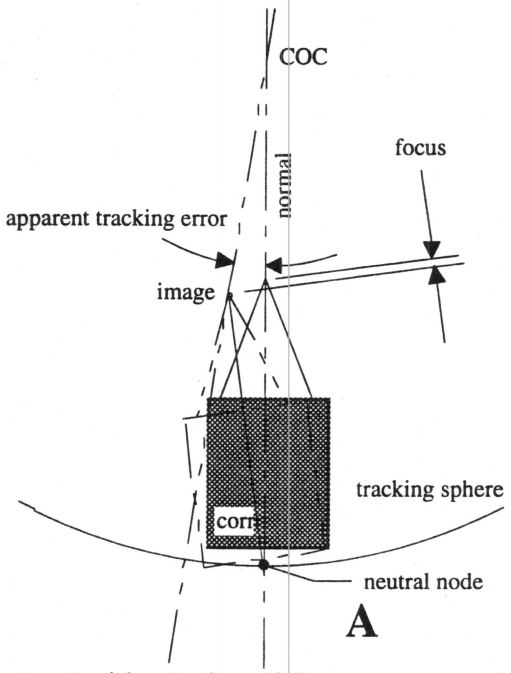

Figure 7a. Correcting a tracking error with rotation of the corrector optics about the coma-neutral node.

Another strategy to be considered is to rotate the corrector/instrument package about its center of mass (made equivalent to the point **RP**), which would be tracked by adjusting the radius $\mathbf{F}_S$ to fit that point, and then making real-time pointing corrections about the coma-neutral node. As will be seen,

tracking the coma-neutral node implies a significant mass offset and therefore a moment to be countered by passive stiffness in the lower (**XY**) stages resulting in an inevitable pointing error. Cartesian tracking of the center of mass introduces no such moments, and coma-neutral rotations for pointing correction, which must be limited to 7 arc seconds as argued above, will introduce very small pointing errors due to mass offsets.

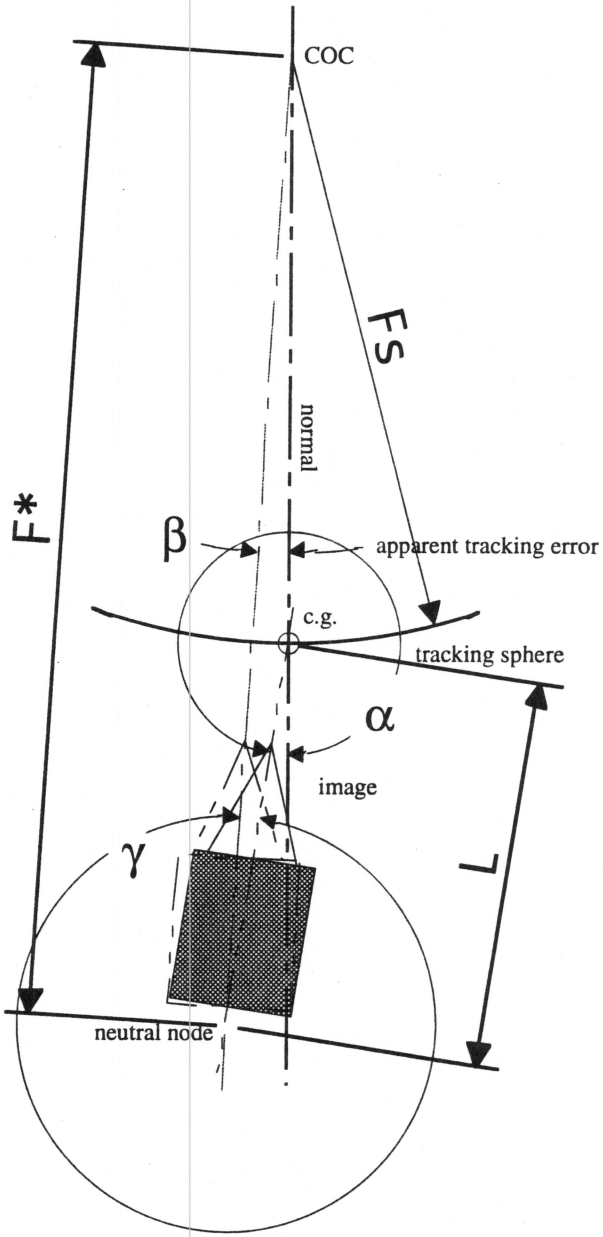

Figure 7b. Correcting a tilt error with rotation of the corrector optics about the coma-neutral node.

As can be seen in figure 7b, when L is the distance from the rotation point to the coma-neutral node, and **F*** is the radius from COC to the neutral node, then for small angles $\beta = L\alpha/\mathbf{F}^*$, where α is the error in optics rotation about a point such as the instrument c.g., and β is the apparent error on the sky. Similarly, the rotation about the neutral node required to correct for the best image is $\gamma = L\alpha/\mathbf{F}_S$. The "leverages" $L/\mathbf{F}^*$ and $L\mathbf{F}_S$ are similar in size and may be used to set the accuracy and resolution of servo actuators used to tilt the prime focus instrument package.

8. Tracking error considerations

Pointing errors larger than 0.6 arc seconds are not within the range of coma-neutral rotation of the corrector and may indicate

(1) an incorrect value for the primary mirror's radius of curvature (hence, for $\mathbf{F}_S$),

(2) an incorrect azimuth reading (can also be due to errors in roll and pitch)[5],

(3) an incorrect value for δ_c (TDE),

(4) unmodeled flexure or tilt in the tracker, or

(5) an incorrect parallactic angle setting.

Discrimination between these error types may require significant traversal of the trajectory **m** to identify the principal contributing variables.

Open loop tracking error E_{OLT} determines the accuracy and resolution required for the multi-axis servomechanism thus far suggested. If we subdivide the allowable Cartesian error into 3 parts, EX, EY, and EZ, where EX and EY are directly related to the XY coordinate system of the gantry mechanism (in arc seconds), and EZ is scaled by $\left(\frac{\pi}{2} - \tan^{-1}(f/N)\right)$, because tracking errors in Z produce mostly a focus effect, then the condition that

$$\sqrt{2\,EX^2 + 2\,EY^2 + EZ^2} \le E_{CAR} \tag{45}$$

helps to define a distribution of the error among the 3 Cartesian axes. One such distribution, where EX = EY = 0.011mm and EZ = 0.015mm produces an E_{CAR} (RSS) of 0.51 arc seconds. Finally, the RSS of E_T, the tilt error budget about the coma-neutral node, and E_{CAR} must be less than the error for open loop tracking (E_{OLT}); if we allow 0.5 arc seconds for E_T the total for the tracking error budget is

$$\sqrt{E_T^2 + E_{CAR}^2} \le E_{OLT} = 0.71 \text{ arcsec.} \tag{46}$$

Tilt table or hexapod legs acting on a baseline of B mm will require an accuracy of k E_L to maintain a tilt error budget of E_T arc seconds, where k is some leverage factor. The error budget for E_L in mm is related to B and E_T by the equation

$$E_L = \frac{\sqrt{3\,E_T^2\,B}}{206265} \tag{47}$$

so that k E_L evaluates to about 0.02 mm when B ≈ 433 mm (derived from 3 equally-spaced kinematic points on a 500 mm radius and k = 10); roughly the same order as that allowed for the focus term (.015 mm) on the hexapod legs.

9. Accuracy, range, and resolution of servo subsystems

A rectangular Cartesian gantry robot for the SST must cover a 12° square section of the tracking sphere whose radius, for the coma-neutral node tracking strategy, will be about 26165 - (12911 - 45) = 13299mm[6]. Allowing for design changes of 2% (132mm), we can say that a maximum tracking sphere radius $\mathbf{F}_S$ would be 13,600mm. The 12° square must rotate through all parallactic angles, so that in order for the **XY** mechanism to cover it, the angular range must be the length of the angular diagonal, $12\sqrt{2}$ ° ≈ 17°. In the XY plane, this projects to 2 $\mathbf{F}_S$ sin (8.5°) = 4020.4mm. A closed-loop linear resolution of 0.005mm provides 0.005/$\mathbf{F}_S$ radians = 0.08 arc seconds on the sky. The maximum rate will occur when slewing or retracting the mechanism. If set at 1.0 in./sec., this gives a maximum slewing time of 158 seconds, or about 3 minutes, allowing for reasonable acceleration and deceleration. We can thus list the following:

---

5 F. B. Ray, "SST pointing error tolerances", SST Technical Report TR-083, February, 1992

6 P. MacQueen has established the vertex of a baseline corrector's #3 mirror at 12911mm from the primary mirror vertex, based on a primary mirror radius of curvature of 26165mm, in "SST Optical Report", SST Technical Report TR-055, summer, 1991..

X and Y axes

Linear absolute accuracy (open loop): ±0.001 in. (±0.025 mm)

Range: 158.28 in. = 4020.4mm

Linear resolution (closed loop): ±0.0002 in. (±0.005 mm)

Rates: Continuously variable (and reversible) 0 to 1.0 in./sec.

Hexapod Legs

For a hexapod mechanism, which must supply the angular offsets, focus, and field rotation for the corrector optics and prime focus package, we may derive similar specifications. The maximum extension of the (SST) hexapod legs occurs in the north (azimuth = 0°), at 70.7° declination and at the very limit of the gantry travel, HA = 18.44° (see figure 17b). At this extreme $\theta = 5.95°$ and $\phi = 6.03°$. Field rotation at this limit is at a maximum of 17.37°.

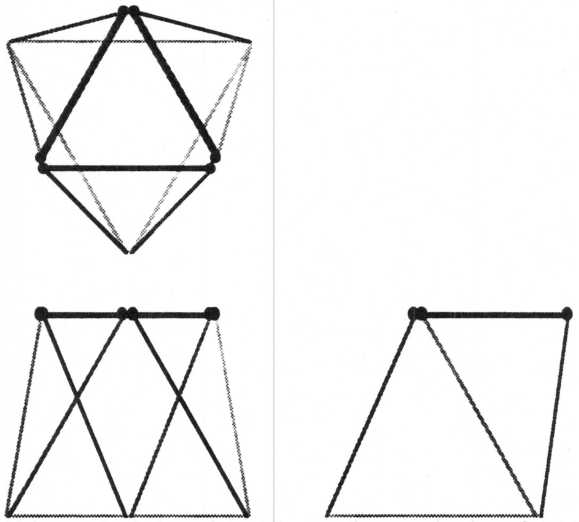

Figure 8. Hexapod geometry assuming a height of 1000mm, base circle of 1400mm dia., upper circle of 1000mm dia., lower mechanical points at 31°, 149°, 151°, 269°, 271°, and 29°, and upper mechanical points at 87°, 93°, 207°, 213°, 327°, and 333°. The legs H1-H6 are labeled in a counter-clockwise sense beginning from the upper right in the top view. The heavier lines are in the movable plate's plane. No transformation has been applied to the movable plate ($\beta = 0$).

To calculate the leg extensions and other specifications for a particular hexapod we assume a 500mm bolt radius for the mounting of the legs to the (upper) movable plate, a somewhat larger bolt radius of 700mm for the mounting of the legs to the (lower) fixed plate (see figure 8). We assume nominal angular spacings on the fixed plate of 30°, 150°, and 270°, and on the movable plate of 90°, 210°, and 330°. Assuming 6 points per circle, we also assume symmetrical disposition of 3 pairs of points per plate, using 1° tangential offsets from the nominal angles mentioned above on the fixed plate, and 3° tangential offsets from the nominal angles mentioned above on the movable plate . On the fixed plate, we therefore have mechanical points at 31°, 149°, 151°, 269°, 271°, and 29°, and on the movable plate, at 87°, 93°, 207°, 213°, 327°, and 333°, in respective (connective) order. The plates are assumed to be 1000mm apart when $\beta = 0$.

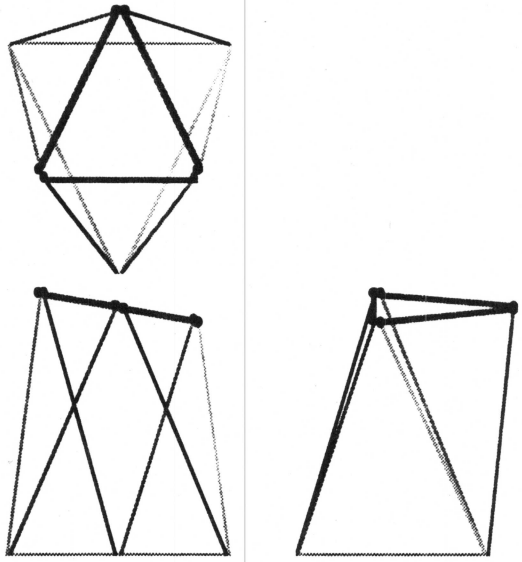

Figure 9a. Hexapod with a tracking rotation applied about the center of the movable plate.

Figure 9a illustrates a pure rotation at a tracking limit which will be encountered in the SST where $\theta = 0.10^\circ$ and $\phi = 8.41^\circ$ assuming a rotation about the center of the hexapod's movable plate. This occurs at the East end of the trajectory when $\mathbf{A} = 24^\circ$, $\delta_T = 65.5^\circ$, at the maximum "reach" of the tracking square (see figure 9b). The parallactic angle in this case $\approx 45^\circ$, which means the trajectory can be followed to the limits of the XY stage. To use this type of tilt correction, we would be tracking the plate center in XYZ, and radius $\mathbf{F}_S$ would be adjusted accordingly. The 6 leg extensions to achieve this rotation are plotted in figure 10.

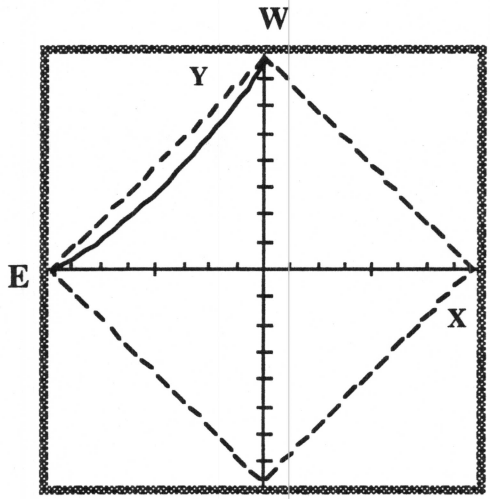

Figure 9b. Trajectory at the limit of the 6° field when A=24°, $\delta_T = 65.5^\circ$. The heavy lines represent the limits of the XY tracking stage.

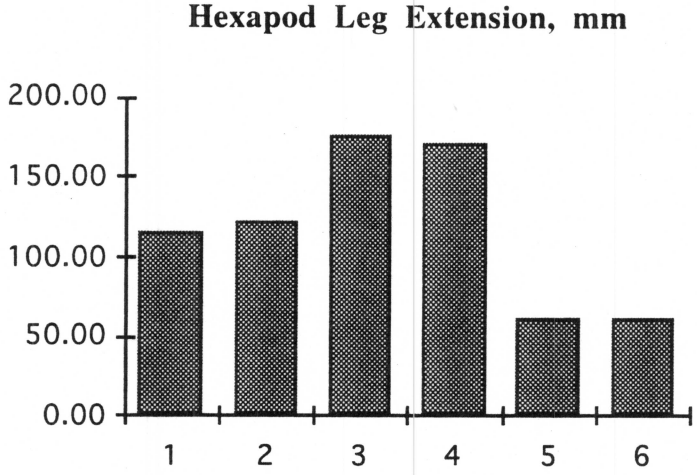

Figure 10. Hexapod leg extensions for the central rotation illustrated in figure 9a.

Assuming the coma-neutral node is 515mm below the movable plate, we may also apply the same rotation ($\theta = 0.10^\circ$, $\phi = 8.41^\circ$) about the coma-neutral node, as illustrated in figure 11. Close examination of the top (XY) view as compared with figure 9a reveals an offset in X (to the right) of the mass carried by the movable plate. This offset may occur in any orientation, and therefore introduces varying amounts of torque on the XY stage, depending on the parallactic angle.

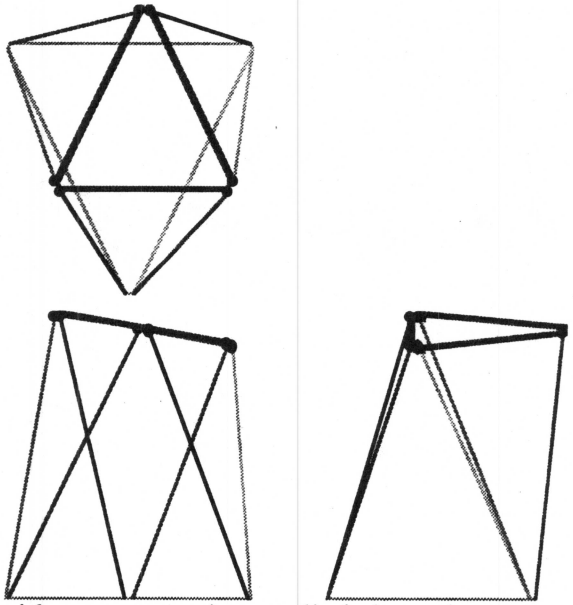

Figure 11. Hexapod with a pure rotation applied about the coma-neutral node.

The range of leg extensions for the coma-neutral rotation, shown in figure 12, are roughly the same as those for central point rotation, indicating only a weak dependency on the point of rotation.

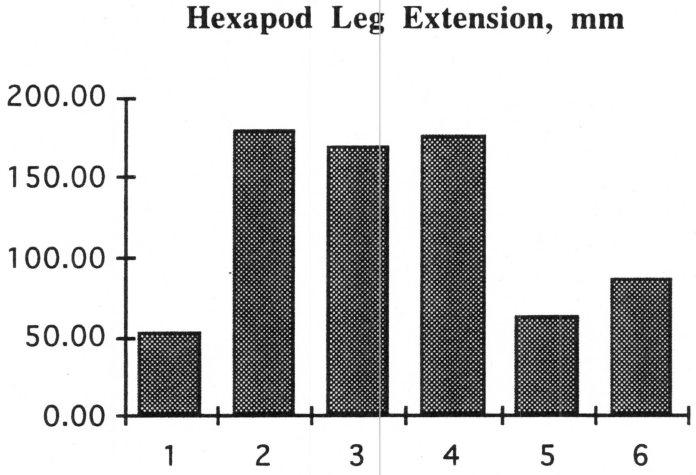

Figure 12. Hexapod leg extensions for a pure rotation applied about the coma-neutral node shown in figure 11.

The hexapod may also correct for field rotation, which in this case will be about 17.37°. Figure 13 illustrates the displacement of figure 11 plus extremal field rotation about the line of sight.

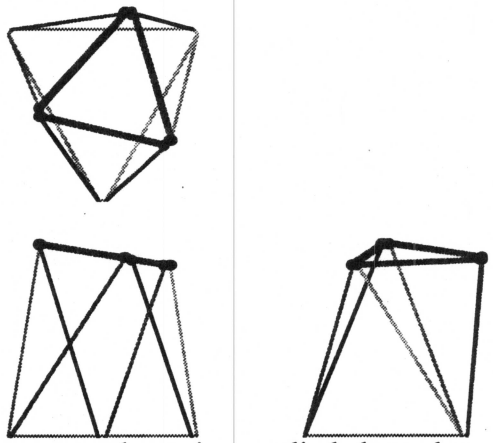

Figure 13. Hexapod excursion for an extremal rotation applied about the coma-neutral node, as in figure 11, plus field rotation about the line of sight.

The top view in figure 13 clearly shows the rotation of the top plate to match the field. What is notable is that the extrema of leg extensions are not greatly increased by including field rotation, indicating that the field rotation mode of the hexapod is available at no extra cost, and that the overall parallactic angle "setting" accomplished by a rotary stage can perhaps be made with less precision than it would need if it were also called upon to track field rotation. Figure 14 plots the hexapod leg extensions for figure 13.

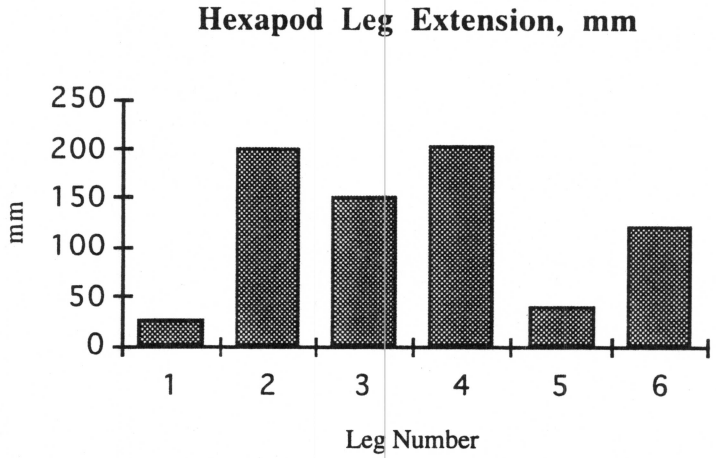

Figure 14. Hexapod leg extensions for the extremal rotation shown in figure 13, which includes field rotation about the line of sight.

To explore the strategy of rotation about a center of mass, we assume such a center 300mm above the movable plate. About that point, an excursion for $\theta = 0.10^\circ$ and $\phi = 8.41^\circ$ plus field rotation (-13.26°) is applied and illustrated in figure 15. The lateral offset in the top view is the motion necessary by the movable plate to achieve this more balanced rotation. Coma-neutral rotation of about 7 arc seconds may be added to this for pointing and guiding corrections. Leg extensions for rotation about the assumed c.g. are illustrated in figure 16. Note that leg extension is dominated by Z tracking rather than tilt.

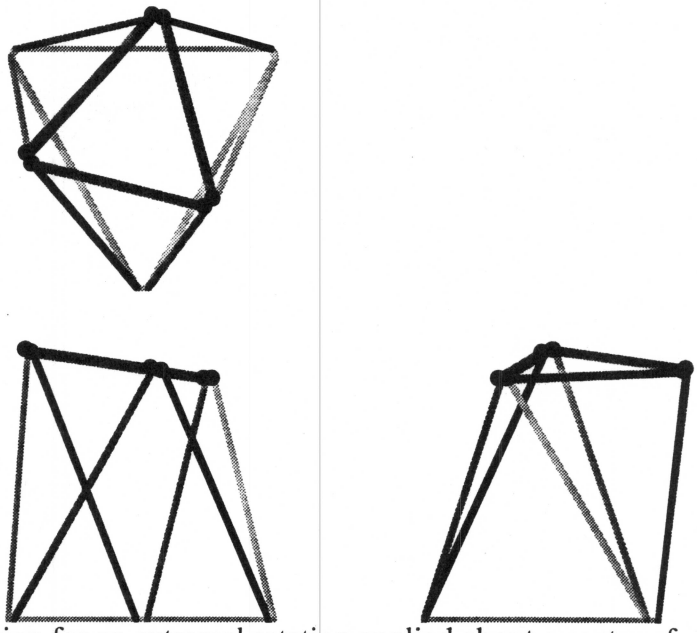

Figure 15. Hexapod excursion for an extremal rotation applied about a center of mass node located 300mm above the movable plate, with tilts and field rotation as in figure 11.

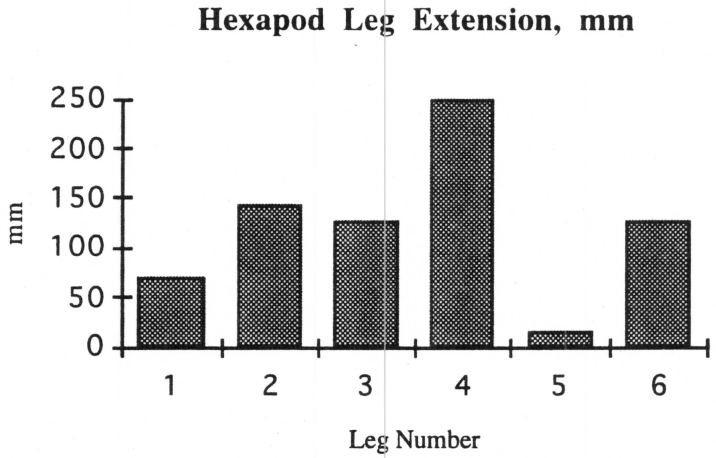

Figure 16. Hexapod leg extensions for the rotation about an assumed center of mass as shown in figure 15, which includes field rotation about the line of sight.

For this case, illustrated in figure 16, the maximum leg extension is 250mm.

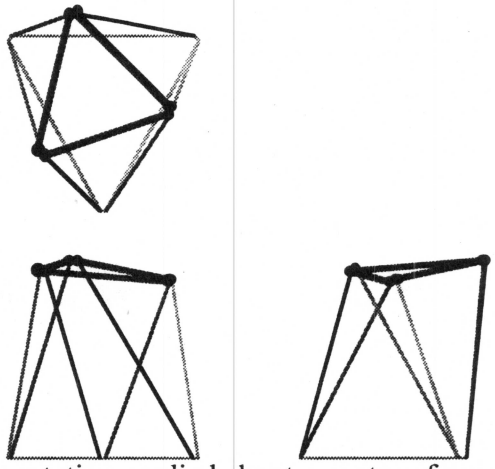

Figure 17a. Hexapod excursion for a rotation applied about a center of mass node located 300mm above the movable plate, with tilts commensurate with $\mathbf{A} = 0°$, $\mathbf{h_c} = -18.44°$, $\delta_T = 70.7°$, i.e. $\theta = 5.95°$, $\phi = 6.03°$, *extreme* field rotation = 17.37° (see figure 17b).

Maximum leg extension occurs in the case of figure 17 (at the East or West ends of the trajectory in figure 17b), (when $\mathbf{A} = 0°$, $\mathbf{h_c} = -18.44°$, $\delta_T = 70.7°$, i.e. $\theta = 5.95°$, $\phi = 6.03°$, field rotation = 17.37°), and is illustrated with hexapod rotation about an assumed center of mass in figure 17a, with leg extensions diagrammed in figure 18.

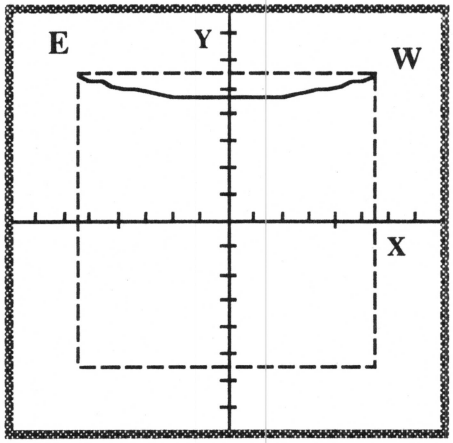

Figure 17b. Trajectory at the limit of the 6° field when A=0°, δ_T= 70.7°. The heavy lines represent the limits of the XY tracking stage.

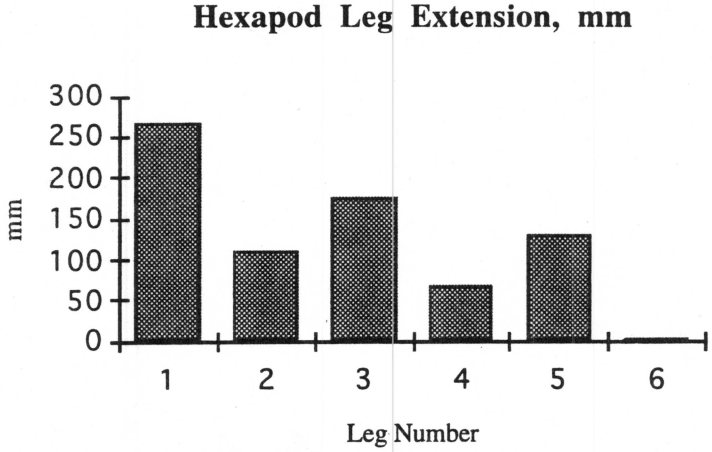

Figure 18. Hexapod leg extensions for the rotation about an assumed center of mass as shown in figure 17, which includes field rotation about the line of sight. The maximum leg extension (H1) is just over 265mm.

A greater leg extension is found when **A** = 0 and we reach the maximum declination possible. Once a definite hexapod design is completed, the complete range specifications may be derived using the above equations. However, it will suffice at this stage to use an extension range of 270mm. It should also be kept in mind that there can be slight negative extensions of the legs in certain situations, and we will allow an additional 30mm for that.

Accuracy and resolution may be established with the aid of figure 19, which plots the maxima, minima, and absolute values of the hexapod, assuming a base radius (denoted by rV in the figure) of 700mm and radii for the movable plate ranging from 500 to 800mm (other dimensions are as previously defined). There is only a slight degree of nonlinearity in any of the curves, and linear arguments and approximations may therefore be substituted. Similar calculations reveal that sensitivity to leg extensions depends mainly on the radius of the mounting points on the movable plate. The hexapod is assumed to have a YZ symmetry plane, and is therefore not symmetric about XZ, hence the sensitivity to leg extensions is slightly different for tilts about X (θ) and Y (ϕ). (Similar plots apply to the wobble plate).

The effect of such tilts on the sky must be evaluated using some de-magnification factor as discussed previously, which depends upon the radius of the tracking sphere and the rotation point chosen for pointing correction. Approximately an order of magnitude gain in sensitivity is available regardless of what points are actually chosen, so the chart may therefore be loosely interpreted as leg extensions required for 0.1 arsecond corrections on the sky.

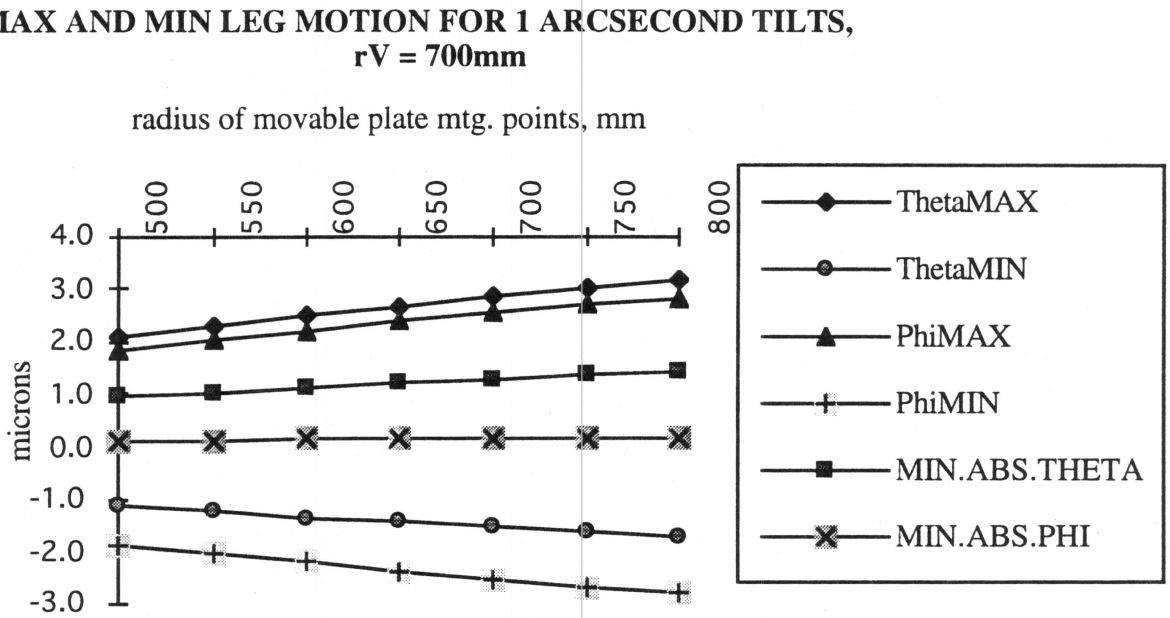

Figure 19a. Hexapod maximum leg extensions for 1 arcsecond tilts of the movable plate about X (θ) and Y (ϕ) for various actuator mounting circle radii. The radius rV of the fixed plate mounting points is 700mm. Very small non-zero extensions must lie within the dead band of the system, and are somewhat dependent on hexapod geometry.

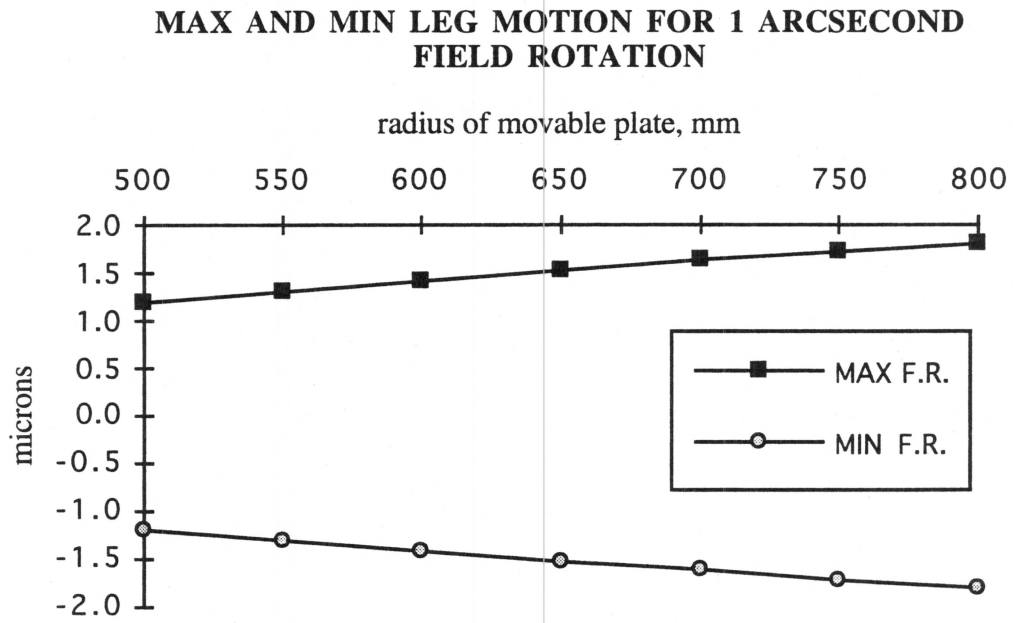

Figure 19b. Hexapod maximum leg extensions for 1 arcsecond field rotation of the movable plate about the line of sight for various actuator mounting circle radii. The radius rV of the fixed plate mounting points is 700mm. Rotations of this nature contain an antisymmetry of leg motion, so that both max. and min. values are exercised in any rotational excursion.

Hexapod leg rates

The entire range of 300mm must be covered in the slewing time of 2.5 minutes, giving a maximum rate of 2 mm/sec. However, in this mode, slewing to the next "start of trajectory", the precision of motion is relatively unimportant. For the hexapod, of course, there is a need to orchestrate the 6 leg retractions with a series of well-defined matrix multiplications in order to avoid developing problematic stress in the movable plate. Most modern control systems contain interpolation codes which allow just a few control points to control such a movement, and since the precision of motion while slewing is unimportant, the control system can interpolate the intermediate points to satisfy the low stress condition. It remains to be seen how few trajectory control points will suffice. Slewing may be accomplished with a basically linear trajectory for maximum efficiency and speed.

In general, as more exact designs become available, further modeling and system simulation can refine the specifications estimated here.

A previous study has established the specification for a rotating stage which carries a prime focus instrument. If this is used to establish the parallactic angle, an immediate correction can be made once the field is acquired, using the hexapod for example. The ρ axis is only weakly coupled to the other axes, and its error in setting can be computed immediately from off-axis image positions. The previous specs. are quoted below.

Parallactic angle (p axis)

Rotating ring, 1m O.D.

Range: 190° min. (see the discussion of parallactic angle)

Angular absolute accuracy (open loop): ± 1 arc minute

Rates: 0 to 3°/sec., continuously variable

Parallactic angle (rotating stage) slewing will not normally occur unless there is an azimuth change, except when used on top of the wobble plate, where it will slew to the next field rotation position. The extreme range for this type of slew is less than 16.5°. When setting in azimuth, the parallactic angle can change as much as 360°, and would therefore have a similar slew rate.

10. Servo layout and simulation

System complexity for the SST's multi-axis tracking device makes it unlikely that an explicit transfer function will be generated via Laplace or z transform methods as is commonly done with single DOF control systems. Therefore, modal finite element methods are needed to establish a state space transition matrix which can then be incorporated into a control simulation software environment.[7] There, the specifications, performance, and control software may be further developed. Issues such as distribution of the control algorithm may be considered with an example of software design which will be very close in size and concept to the final SST program set. Locally, however, the axes may be controlled with linear techniques. Examples of such simulation environments are Simula by MATLAB, Inc. and SystemBuild from Integrated Systems, Inc.

---

7 S. Morrsion & J. Caffrey, "Description of an interface between MSC/NASTRAN and MATRIX$_x$ with example applications", Integrated Systems, Inc., April 23. 1991.

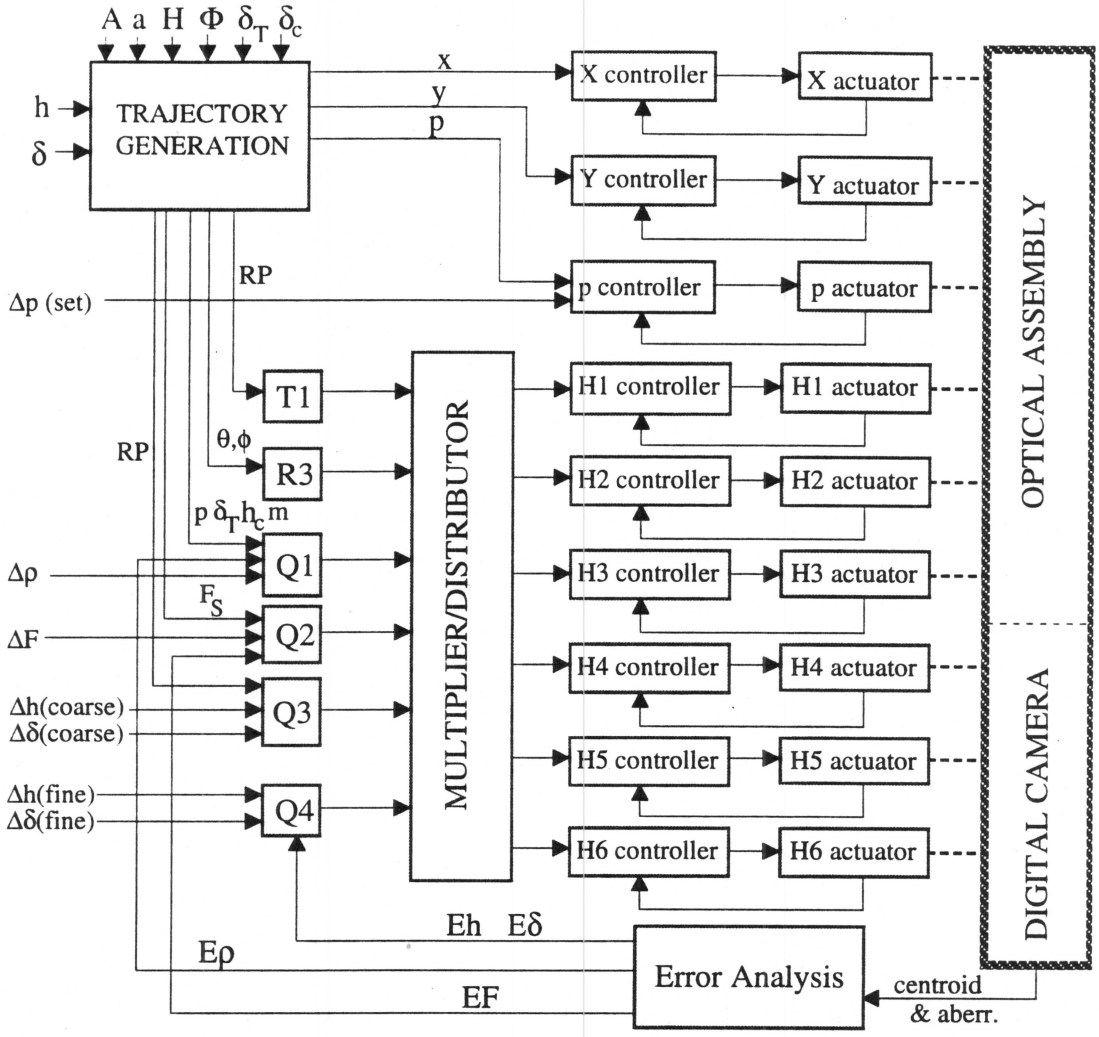

Figure 20. SST tracking servo (XYp+hexapod). Three major software blocks are shown at this level.

Top-level software design and implementation

The tracker control system lends itself to object-oriented and dataflow programming software methodology. Recent developments in high-level systems which visually implement object-oriented programming paradigms may be useful in developing the system and enhance code production rates. There is a large percentage of parallelism in the device, and this should naturally be incorporated into dataflow software, where parallelism is an implied benefit. Similar visually-oriented systems are available for the controller design, and, when coupled with finite element modal analysis, will help to design a straw man controller at about the same rate as the machine design progresses.

An overall top-level servo design, shown in figure 20, takes advantage of the de coupling possible using a hexapod device by means of a separate multiplier/distributor code module where time-dependent, hand paddle, and autoguiding corrections may be processed. The dotted lines at the right side of the figure indicate mechanical connections to the driven optical assembly. A tracking/acquisition camera provides output for the overall feedback loop. Software matrix processors T1, R3, Q1, Q2, Q3, and Q4 adjust the pre multipliers of points on the movable hexapod plate. The multiplier/distributor calculates the hexapod leg positions and distributes them to the controller set. All pre-multiplier matrices are expressed in homogeneous coordinates and are 4×4 in size. Each matrix processor will collect a few matrix factors which are multiplied together to send to the multiplier/distributor. Part of the distributor (computing leg lengths) may be accomplished concurrently in each controller's software.

The fundamental time-dependent trajectory is generated by a separate code segment, feeding the **XY** stage an independent set of coordinates. Inputs include **H** (distance of the telecentric axis from the

meridian), Φ (latitude), δ_T (distance from the transit point to the equator), and δ_c, distance from the telecentric axis to the equator), and the time-dependent variables **h** (hour angle) and δ (declination). Parallactic angle **p**, which may be held constant (clamped) during tracking if the hexapod provides field rotation, can also be output from this module, although setting corrections are possible as inputs to the **p** controller. The **X** and **Y** controllers may split into slaved servos to avoid racking and may include preload and counterbalance motors.

Metrology information, which typically varies slowly, can also be added as input to the trajectory generation module, whenever its variables are defined.

Feedback of an image centroid for pointing corrections and aberrations which may be obviated by corrective optical tilts and/or focus are filtered, scaled, and distributed by an error analysis routine which accepts and processes image data from a digital camera rigidly mounted to the optical assembly. Controller modules may require crosstalk processing, some of which may be predictable using state-space modeling and simulation methods supplemented by a dynamic finite element analysis of the tracker's physical design.

Operator hand paddle and systematic guiding corrections supply real-time adjustments to the matrix factors. Therefore, multiplication and distribution for a hexapod controller can reside in the controller module only if there is sufficient memory. An analysis of some straw man algorithms should be sufficient to determine whether this is feasible. If not, the code can reside in the tracking sub-system (TS) computer, and appropriate communication lines to the controllers anticipated. Partitioning of the operations may be accomplished by defining the appropriate family of processes for a (real-time) operating system in the TS computer.